

Article

Distribution of As within Magnetic and Non-Magnetic Fractions of Fluidized-Bed Coal Combustion Ash

Filip Kovár and Lucie Bartoňová * 

Department of Chemistry, Faculty of Materials Science and Technology, VŠB—Technical University of Ostrava, 17. Listopadu 15, 708 00 Ostrava, Czech Republic; filip.kovar.st@vsb.cz

* Correspondence: lucie.bartonova@vsb.cz; Tel.: +420-596-991-514

Abstract: Separation of coal ash into magnetic and non-magnetic fractions facilitates their utilization when processed separately. Due to desulphurization additives added to coal during the fluidised-bed combustion, non-magnetic fractions often contain elevated CaO levels (while magnetic concentrates are typically rich in Fe₂O₃). Both CaO and Fe₂O₃ are known for their ability to bind As during the combustion, whose distribution is a crucial parameter in terms of proper utilization of these fractions. Therefore, the study deals with the As partitioning within magnetic and non-magnetic fractions of fluidized-bed coal combustion ashes. Two different (successive) procedures of dry magnetic separation were used to separate each ash into strongly magnetic, less magnetic, and a non-magnetic fraction. Due to their optimal utilization, the concentrations of As and other target elements in these fractions were evaluated and compared. Magnetic concentrates from the first separation step (in vibrofluidized state) contained 60–70% Fe₂O₃, magnetic concentrates separated manually out of the residues after the first separation contained 26–41% Fe₂O₃, and the non-magnetic residues contained 2.4–3.5% Fe₂O₃. Arsenic levels were the highest in the non-magnetic residues and gradually decreased with the increasing Fe₂O₃ content in the magnetic fractions. The dominant As association in the studied samples was to CaO ($r = +0.909$) and with SO₃ ($r = +0.906$) whereas its joint occurrence with Fe₂O₃ was improbable ($r = -0.834$).

Keywords: coal combustion; arsenic; desulphurization; additives; retention; CaO; Fe₂O₃



Citation: Kovár, F.; Bartoňová, L. Distribution of As within Magnetic and Non-Magnetic Fractions of Fluidized-Bed Coal Combustion Ash. *Minerals* **2021**, *11*, 1411. <https://doi.org/10.3390/min11121411>

Academic Editors: Shifeng Dai and David French

Received: 27 October 2021
Accepted: 8 December 2021
Published: 13 December 2021

Publisher's Note: MDPI stays neutral with regard to jurisdictional claims in published maps and institutional affiliations.



Copyright: © 2021 by the authors. Licensee MDPI, Basel, Switzerland. This article is an open access article distributed under the terms and conditions of the Creative Commons Attribution (CC BY) license (<https://creativecommons.org/licenses/by/4.0/>).

1. Introduction

Coal has long been a reliable energy source and currently, it is also intensively studied as the source of critical elements, such as REE and Y [1,2]; Ge and Ga [3–5]; Li [6]; Nb [5,7]; U, Se, and Re [6]; or Ta, Zr, and Hf [7]. However, due to the presence of minor and trace elements, it can be responsible for serious pollution problems [8–11]. In general, during coal combustion, minor and trace elements are redistributed among bottom ash (BA) or slag, fly ash (FA), and emissions. Redistribution among these coal combustion products is determined by the operational conditions [12,13], coal characteristics [14,15], co-combustion of coal with wastes [16–18], or addition of desulphurization additives [19,20].

Coal combustion is still the main anthropogenic source of As, a toxic and volatile element with potential carcinogenic properties and bioaccumulation tendency in the environment [21]. The average concentration of As in world lignite and bituminous coal is 7.4 and 9.0 ppm, respectively [22]. The shares of As in bottom ash, fly ash, and emissions vary considerably depending on the total ash distribution, combustion temperature, amount and type of desulphurization additive, overall composition of the ashes, and flue gas and type (and working temperature) of the particulate control device. However, since As is quite volatile, its share in emissions is not generally negligible.

The release of As into the environment relates not only to emissions (in the finest fly ash particles or emitted in gaseous form) [11], but is also connected with its presence in coal combustion ashes. Namely, in fly ash, arsenic could be highly enriched [3]. Power stations produce a vast amount of solid wastes annually; therefore, the reuse of these wastes not

only produces valuable components but also facilitates mitigation of the problems with waste storage/disposal [23].

Magnetic separation is widely used for ash separation into two basic components: magnetic and non-magnetic fractions [24,25] (the latter can be even further classified by chemical methods [26]), thereby facilitating utilization of these fractions if processed separately (e.g., non-magnetic fraction as a concrete component [27] and the magnetic one as a substitution of natural magnetite in dense medium (coal) cleaning applications) [28,29].

Typical components of non-magnetic fractions of fluidized-bed combustion ashes are Ca-bearing minerals (in addition to aluminosilicates and quartz), while in the magnetic fractions, Fe_2O_3 typically prevails. Since both CaO [30–33] and Fe_2O_3 [34–37] can bind (and accumulate) As [38–43] during coal combustion, its distribution within these two fractions is crucial in terms of ecological utilization of magnetic concentrates and the non-magnetic residues.

Circulating fluidized-bed combustion is a modern technology. In comparison to PCC, it is advantageous due to its high combustion efficiency and low NO_2 and SO_2 emissions [44–47]. It is worth mentioning in this context that the presence of Ca-bearing additives (preferentially used for desulphurization) is also beneficial for the retention of As, thereby decreasing its emissions [48]. However, even if the levels of Fe-bearing minerals in fluidized-bed combustion ashes are typically lower (than those of CaO), they can also accumulate As [36].

Therefore, this study deals with the As partitioning within magnetic and non-magnetic fractions of fluidized-bed coal combustion ashes. For detailed elucidation, two different (successive) procedures of dry magnetic separation were used to separate each sample into strongly magnetic, less magnetic, and non-magnetic fractions. With the view of their optimal utilization, the concentrations of As and other target elements in these fractions were evaluated and compared in order to reveal As associations.

2. Materials and Methods

Bottom ash (BA) was collected at an atmospheric circulating fluidized-bed power station, where bituminous coal was combusted with dry desulphurization additive at an approximate temperature of 850 °C. Ash samples were collected at regular time intervals and after mixing, ca. 3–5 kg samples were set apart for laboratory study by quartering. From these bulk ash samples, 3 particle-size fractions were prepared on sieves (when dry): <0.2, 0.2–0.4, and >0.4 mm.

In order to simulate industrial separation into highly magnetic, less magnetic, and non-magnetic fractions, magnetic fractions were separated by a two-step procedure from these 3 particle-size fractions: (i) first, in a vibrofluidized state and then (from the residue after the first separation), (ii) manually using a hand-held magnet. Separation in the vibrofluidized state removed highly magnetic particles while the separation with the hand-held magnet removed less magnetic grains (that was not retained during vibrofluidized separation). Both separations were conducted from the dry sample to avoid leaching of the studied elements.

The concentrations of the target elements in the aforementioned samples were determined by a wavelength-dispersive X-ray fluorescence spectrometer ARL PERFORM' X with 4200 W X-ray tube (Thermo Fisher Scientific, Ecublens, Switzerland) using 12 certified reference materials from China, the USA, and the EU. Mineral phases were identified by means of a Rigaku SmartLab X-ray diffractometer (with a $\text{CoK}\alpha$ X-ray tube) (Rigaku, Tokyo, Japan).

Correlation coefficients (and their statistical significance) were calculated using QC. Expert 3.3.0.7. program (TriloByte Ltd., Pardubice, Czech Republic).

3. Results and Discussion

3.1. Composition of Ashes and Their Magnetic/Non-Magnetic Fractions

3.1.1. Chemical Composition of the Studied Fractions

Two-step (dry) magnetic separation of BA was conducted to differentiate between Ca- and Fe-associated As. The results of the chemical analysis of the three particle-size fractions of the studied BA and their magnetic concentrates and non-magnetic residues are summarized in Table 1 as well as the percentage yields of these fractions. The concentrations of As, CaO, and Fe₂O₃ are plotted (for easier evaluation) in Figure 1.

Table 1. Concentrations of the studied elements in magnetic concentrates and non-magnetic residues prepared from three particle-size fractions of BA (MVS = magnetic vibrofluidized state, MM = magnetic manually, NM = non-magnetic).

Particle Size	BA < 0.2			BA 0.2–0.4			BA > 0.4		
	MVS	MM	NM	MVS	MM	NM	MVS	MM	NM
Fraction (wt.%)	0.88	0.89	98.23	0.53	0.64	98.83	1.72	2.48	95.80
As (ppm)	26	39	75	13	56	90	13	25	36
CaO (wt.%)	13.99	26.77	63.62	13.24	30.93	61.48	8.96	10.64	45.02
Fe ₂ O ₃ (wt.%)	60.36	33.32	2.42	62.82	26.70	2.82	70.37	40.31	3.45
SiO ₂ (wt.%)	11.16	17.31	4.50	10.46	19.22	7.29	7.78	25.84	23.12
Al ₂ O ₃ (wt.%)	6.73	10.08	2.51	6.87	11.80	4.02	5.16	13.44	12.10
MgO (wt.%)	1.75	1.52	0.83	1.98	1.59	0.89	1.95	1.60	0.79
K ₂ O (wt.%)	0.37	0.58	0.08	0.29	0.55	0.15	0.20	0.93	0.68
SO ₃ (wt.%)	2.08	6.28	23.97	1.62	6.52	19.99	1.10	2.66	10.62
TiO ₂ (wt.%)	0.53	0.72	0.20	0.56	0.85	0.30	0.46	0.97	0.76

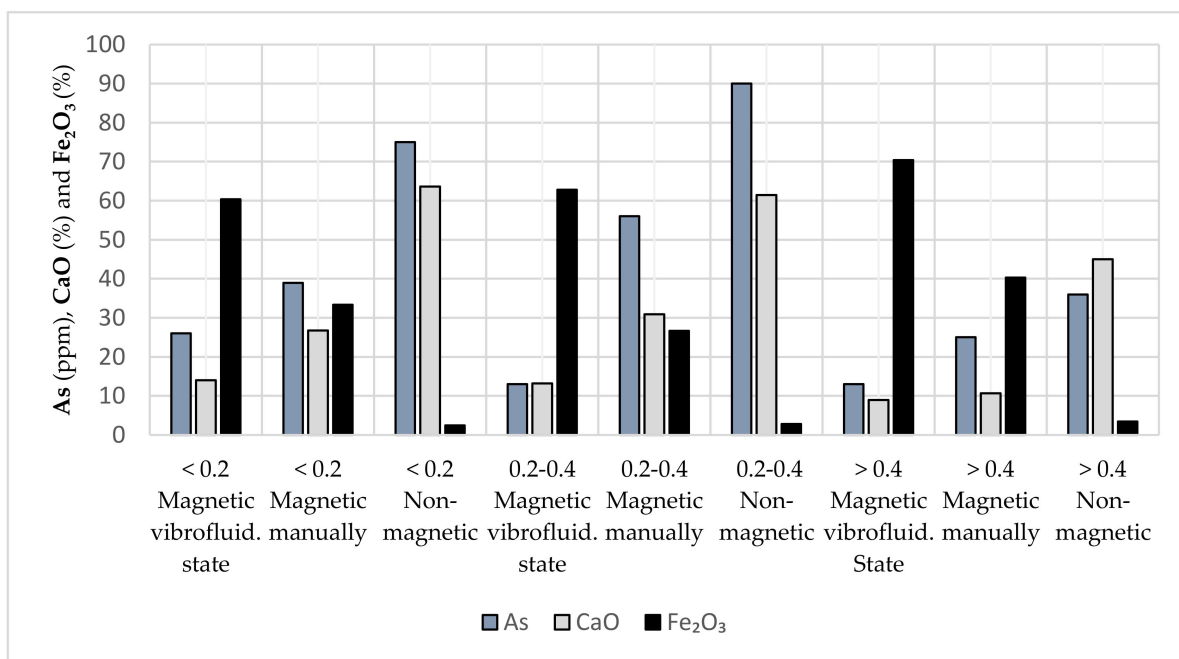


Figure 1. Distribution of As (ppm), CaO (wt.%), and Fe₂O₃ (wt.%) in the particle-size fraction of BA.

Magnetic separation in the vibrofluidized state provides the highest Fe₂O₃ contents (60–70% in all magnetic concentrates); the manual separation applied on the residue after the first separation provided a concentrate with lower purity (26–41% Fe₂O₃) because the particles with a higher Fe content were already removed during the first separation step. The non-magnetic residues contained only 2.4–3.5% Fe₂O₃ after these two separation steps.

Figure 1 (and Table 1) clearly documents the lowest levels of As in the coarsest BA fraction, which is a similar distribution to CaO. In contrast, the levels of Fe₂O₃ increase

with increasing particle size, which is also the case of Si. This trend corresponds with the finely ground desulphurization additive (for efficient interaction with gaseous SO_2/SO_3) and quite large grains with a high SiO_2 content (e.g., quartz particles).

The concentrates originating from the first magnetic separation (in the vibrofluidized state) contain the lowest As and CaO contents while the Fe_2O_3 percentage is the highest in the case of all particle-size fractions. The second magnetic separation (applied to the residue after the first one) provides the magnetic concentrate with a somewhat lower Fe level, which contains moderately higher concentrations of As and CaO. After magnetic separation, the residues (dominantly composed of CaO and SO_3) are enriched in As.

3.1.2. Mineral Composition of the Studied Fractions

Minerals identified in the studied samples are listed (according to their abundance) in Table 2. X-ray diffraction patterns of the magnetic vibrofluidized state, magnetic manual, and non-magnetic fractions of the finest (<0.2 mm) and the coarsest (>0.4 mm) ash samples are depicted in Figures 2 and 3, respectively.

Table 2. Mineral phases identified in the studied magnetic and non-magnetic fractions (MVS = magnetic vibrofluidized state, MM = magnetic manually, NM = non-magnetic).

Particle Size	Sample	Mineral Phases	Particle Size	Sample	Mineral Phases	Particle Size	Sample	Mineral Phases
	MVS	Hematite/ Fe_2O_3 Magnesioferrite/ MgFe_2O_4 Maghemite-Q/ Fe_2O_3 Quartz/ SiO_2 Anhydrite/ CaSO_4 Gehlenite/ $\text{Ca}_2\text{Al}_2\text{SiO}_7$		MVS	Hematite/ Fe_2O_3 Magnesioferrite/ MgFe_2O_4 Maghemite-Q/ Fe_2O_3 Quartz/ SiO_2 Anhydrite/ CaSO_4 Gehlenite/ $\text{Ca}_2\text{Al}_2\text{SiO}_7$		MVS	Hematite/ Fe_2O_3 Magnesioferrite/ MgFe_2O_4 Maghemite-Q/ Fe_2O_3 Quartz/ SiO_2 Anhydrite/ CaSO_4 Gehlenite/ $\text{Ca}_2\text{Al}_2\text{SiO}_7$
<0.2 mm	MM	Hematite/ Fe_2O_3 Magnesioferrite/ MgFe_2O_4 Quartz/ SiO_2 Anhydrite/ CaSO_4 Gehlenite/ $\text{CaAl}_2\text{SiO}_7$ Monticellite/ $\text{Ca}(\text{Mg}_{0.93}\text{Fe}_{0.07})\text{SiO}_4$	0.2–0.4 mm	MM	Hematite/ Fe_2O_3 Magnesioferrite/ MgFe_2O_4 Quartz/ SiO_2 Anhydrite/ CaSO_4 Gehlenite/ $\text{CaAl}_2\text{SiO}_7$ Portlandite/ $\text{Ca}(\text{OH})_2$	>0.4 mm	MM	Hematite/ Fe_2O_3 Magnesioferrite/ MgFe_2O_4 Quartz/ SiO_2 Anhydrite/ CaSO_4 Gehlenite/ $\text{CaAl}_2\text{SiO}_7$ Rutile/ TiO_2
	NM	Portlandite/ $\text{Ca}(\text{OH})_2$ Anhydrite/ CaSO_4 Quartz/ SiO_2 Lime/ CaO Gehlenite/ $\text{Ca}_2\text{Al}_2\text{SiO}_7$ Calcite/ CaCO_3		NM	Portlandite/ $\text{Ca}(\text{OH})_2$ Anhydrite/ CaSO_4 Quartz/ SiO_2 Lime/ CaO Gehlenite/ $\text{Ca}_2\text{Al}_2\text{SiO}_7$ Rutile/ TiO_2		NM	Portlandite $\text{Ca}(\text{OH})_2$ Anhydrite/ CaSO_4 Quartz/ SiO_2 Lime/ CaO Gehlenite/ $\text{Ca}_2\text{Al}_2\text{SiO}_7$ Rutile/ TiO_2

The minerals in Table 2, ordered according to their relevance, suggest similar (nearly the same) mineral compositions in all three magnetic vibrofluidized state fractions, which contain hematite, magnesioferrite, and maghemite (with some admixture of quartz, anhydrite, or gehlenite). Such a composition also corresponds with ca 60–70% Fe_2O_3 in these fractions.

Magnetic fractions separated manually from the residue after the first magnetic separation contain a lower percentage of Fe_2O_3 (26–41%), which is in line with the lower occurrence of Fe-bearing minerals (hematite and magnesioferrite) and greater abundance of other minerals (quartz, anhydrite, gehlenite, rutile, monticellite, and kaolinite). All the residues after the magnetic separations exhibited almost the same mineral composition as well. Since the Fe_2O_3 levels are very low (only a few %), the dominant minerals are those of Ca, Si, or Al (or Ti): portlandite, anhydrite, quartz, calcium oxide, gehlenite, rutile, and calcite.

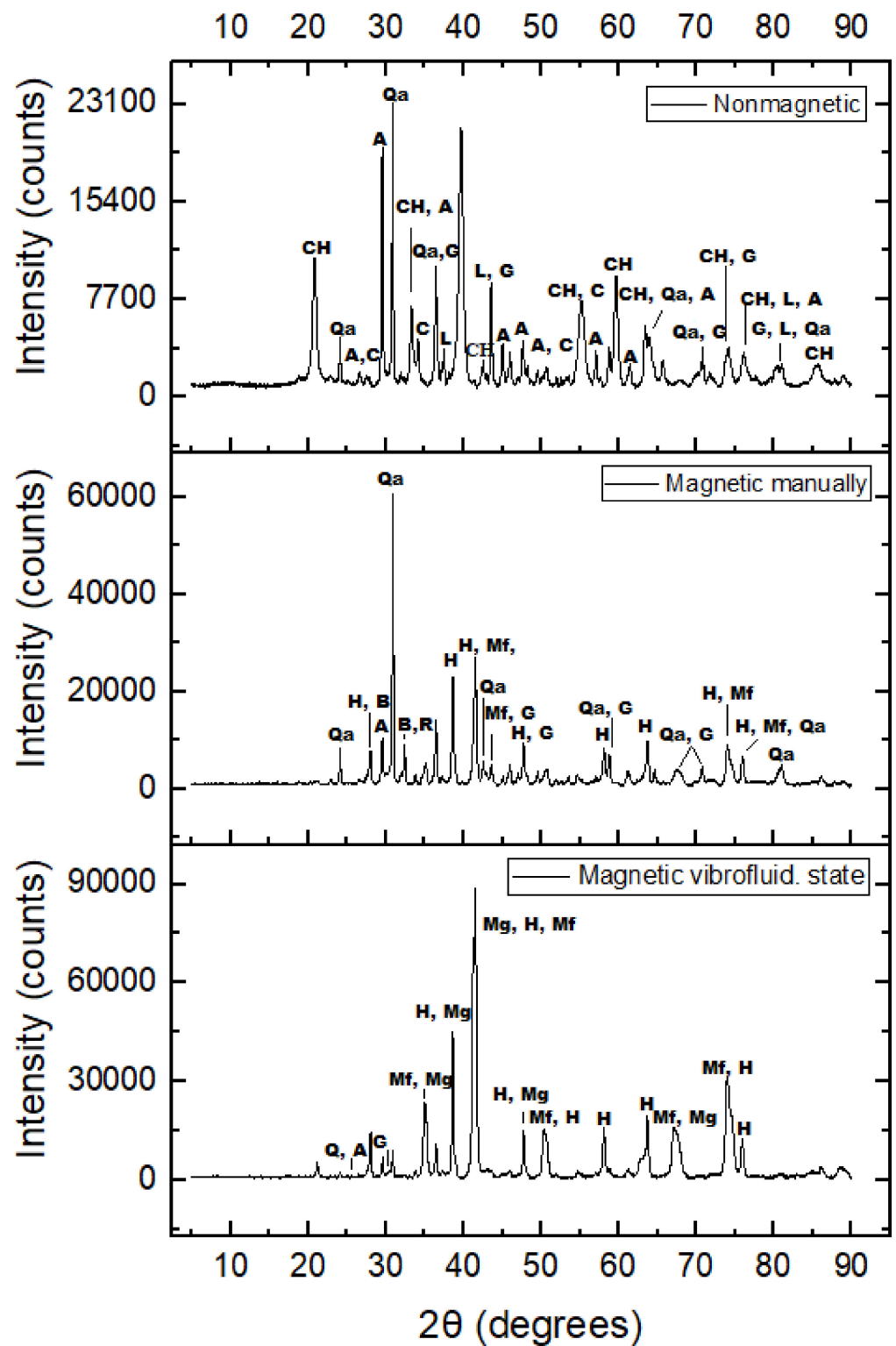


Figure 2. XRD patterns of the magnetic vibrofluid state, magnetic manual, and nonmagnetic fractions of the finest < 0.2 mm (A = Anhydride, B = Bilinite, C = Calcite, CH = Calcium Hydroxide, G = Gehlenite, H = Hematite, L = Lime, Mg = Maghemite, Mf = Magnesioferrite, Q = Quartz, Qa = Quartz alpha, R = Rutile).

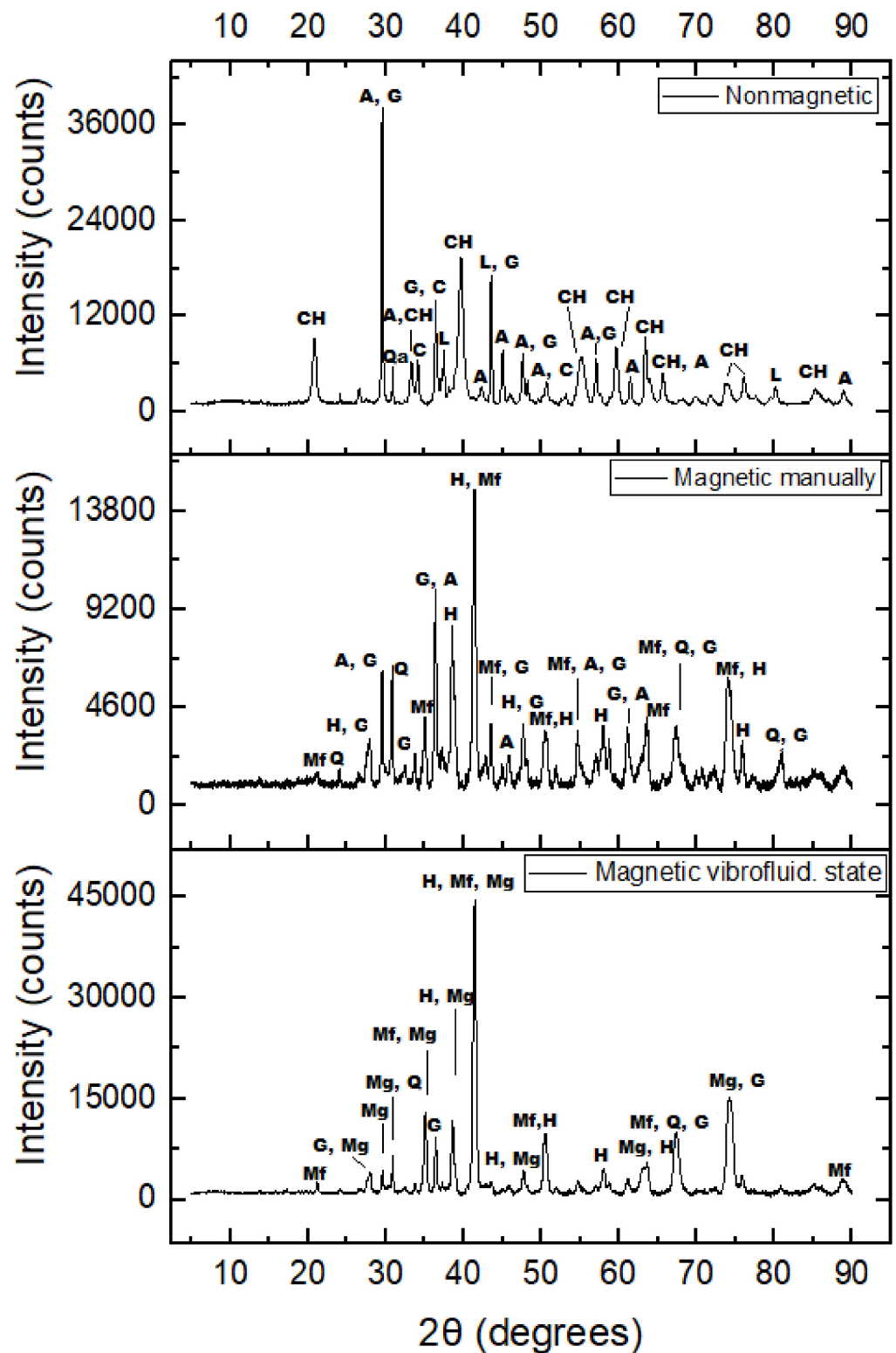


Figure 3. XRD patterns of the magnetic vibrofluid state, magnetic manual, and nonmagnetic fractions of the coarsest > 0.4 mm (A = Anhydrite, B = Bilinite, C = Calcite, CH = Calcium Hydroxide, G = Gehlenite, H = Hematite, L = Lime, Mg = Maghemite, Mf = Magnesioferrite, Q = Quartz, Qa = Quartz alpha, R = Rutile).

3.2. Distribution of As and Target Elements within Magnetic and Non-Magnetic Fractions

3.2.1. Enrichment Factor

For easier evaluation of the overall distribution trends of As and other target elements (expressed in the form of oxides), the *Enrichment factor (EF)* in the magnetic fractions related to the corresponding non-magnetic residues was calculated according to the formula:

$$EF_{(i)} = \frac{w_i(\text{magnetic fraction})}{w_i(\text{non - magnetic fraction})} \quad (1)$$

where the w_i is the weight fractions of the i -th element (or its oxide) in the magnetic or non-magnetic ash fraction. The *EF* values (rounded to two decimals) are summarized in Table 3.

Table 3. Enrichment factors of the studied elements in magnetic fractions (vs. non-magnetic residues).

Particle Size Proceeding of Separation	BA < 0.2		BA 0.2–0.4		BA > 0.4	
	MVS	MM	MVS	MM	MVS	MM
As	0.35	0.52	0.14	0.62	0.36	0.69
CaO	0.22	0.44	0.22	0.50	0.20	0.24
Fe ₂ O ₃	24.94	13.77	22.28	9.47	20.40	11.68
SiO ₂	2.48	3.85	1.43	2.64	0.34	1.12
Al ₂ O ₃	2.68	4.02	1.71	2.94	0.43	1.11
MgO	2.11	1.83	2.22	1.79	2.47	2.03
K ₂ O	4.63	7.25	1.93	3.67	0.29	1.37
SO ₃	0.09	0.26	0.08	0.33	0.10	0.25
TiO ₂	2.65	3.60	1.87	2.83	0.61	1.28

Enrichment factors (calculated according to Equation (1)) are plotted for As, CaO, and S in Figure 4a and Fe₂O₃ in Figure 4b. The same concentrations of the studied element are shown in the magnetic and non-magnetic fractions. Figure 4 suggests that As and CaO (and S) are strongly depleted in all magnetic concentrates, which is even more pronounced in the first (vibrofluidized) separation. As expected, the Fe₂O₃ content is always strongly enriched in the first magnetic concentrates and its enrichment in the concentrate originating from the second separation step is somewhat lower.

3.2.2. Correlations between the Concentrations of the Target Elements

The correlation calculations are used frequently when predicting the content and distribution of elements in coals or combustion residues and for the assessment of their environmental toxicity [48,49]. In order to gain insight into elemental relationships and to evaluate As associations, a correlation matrix was calculated (Table 4). The only statistically significant relationships of As are those with CaO and SO₃ ($r = 0.909$ and 0.906). The correlation coefficient between the contents of As and Fe₂O₃ is negative ($r = -0.834$), revealing a strong inverse relationship. It is interesting in this context that Fe₂O₃ exhibits a strong positive relationship with MgO ($r = +0.960$). The association of As to Al₂O₃ is improbable as well because $r(\text{As}-\text{Al}_2\text{O}_3) = -0.362$. The critical value of the correlation coefficient in this case (for 9 measured values, $\alpha = 0.05$, and two-tailed probability) is $r = 0.666$.

The most interesting relationships are plotted in Figure 5. They are As–CaO, As–Fe₂O₃, As–SO₃, S–CaO, MgO–Fe₂O₃, and Fe₂O₃–CaO. The data listed in Tables 1 and 3 and plotted in Figure 5 indicate a similar distribution of As, CaO, and SO₃ while the distribution of Fe₂O₃ seems to be substantially different (and similar to that of MgO). The aforementioned direct/inverse relationships are in agreement with the mineral analysis results (Section 3.1.2.) documenting an abundant joint occurrence of CaO–SO₃ in anhydrite and MgO–Fe₂O₃ in magnesioferrite. Joint occurrence of CaO–Fe₂O₃ minerals was not identified by X-ray diffraction, which is in line with the inverse relationship.

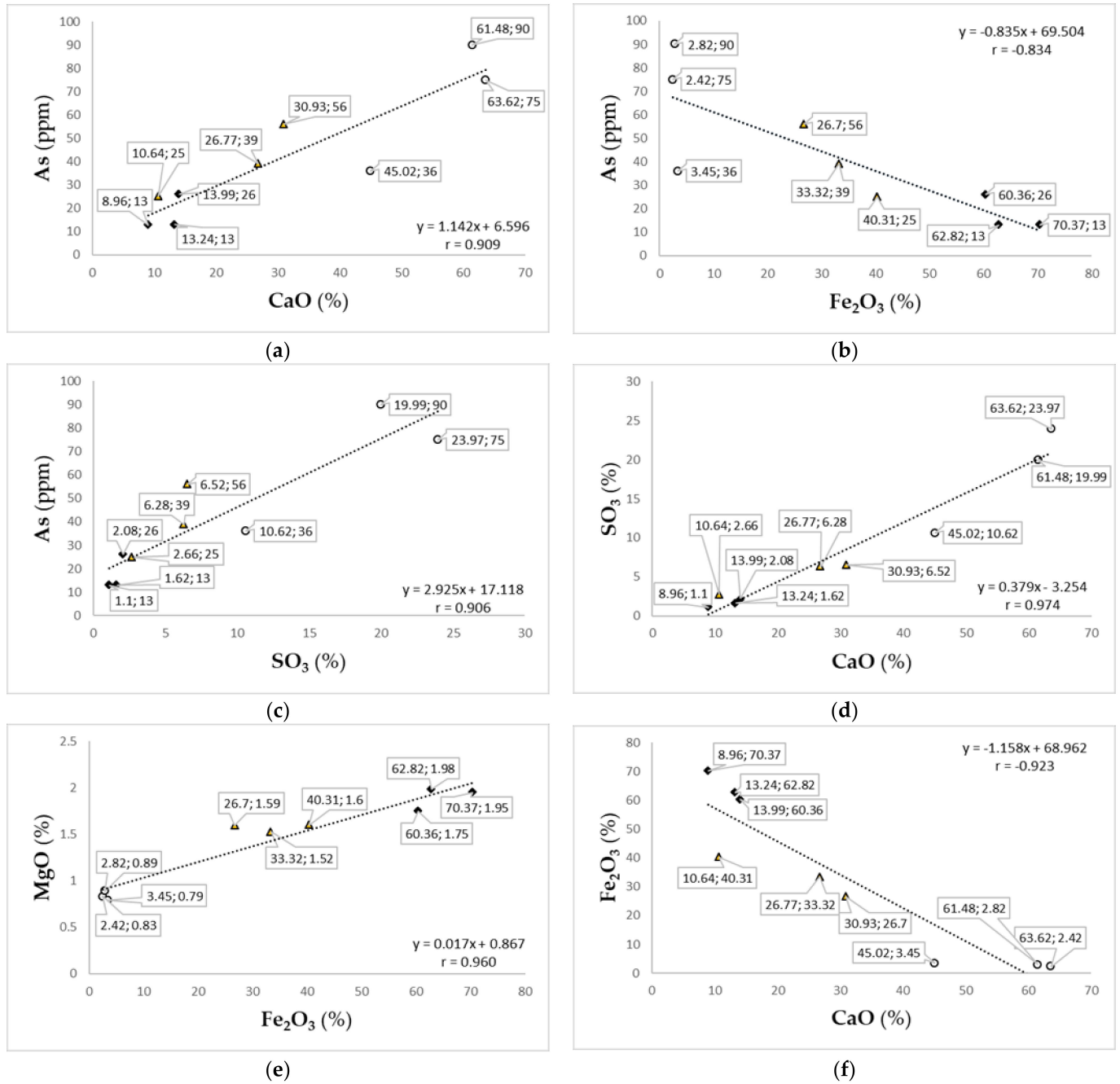


Figure 5. Relationships between the concentrations of (a) As–CaO, (b) As–Fe₂O₃, (c) As–SO₃, (d) SO₃–CaO, (e) MgO–Fe₂O₃, and (f) Fe₂O₃–CaO (black squares are used for highly magnetic fractions, yellow triangles for less magnetic ones, and circles for non-magnetic residues).

Arsenic association with calcareous minerals is in agreement with other fluidized-bed coal combustion results [47,50–54]. Most researchers reported efficient As retention using CaO [52–54]; however, CaSO₄ can also capture As [43,55]. Since the correlation coefficient $r(\text{As-SO}_3)$ is very high as well ($r = +0.906$), the association of As to calcareous sulphates can be expected.

The samples evaluated in this study originated from the coal combustion at ca. 850 °C. According to Zhang et al. [36], ferrospheres separated from coal ash exhibited the best As retention efficiency at 600 °C (ca. 0.55 mg As/g) while at 800 °C, it was only ca. 0.20 mg As/g (i.e., nearly one third) [36]. In the case of CaO, there is still no exact consensus in the literature; nevertheless, higher temperatures seem to promote As retention on Ca-bearing minerals. Li et al. [56] observed an increasing retention efficiency within the temperature range of 400–1000 °C while Chen et al. [55] concluded that the most effective As retention on CaO was at 750 °C. Sterling and Helble [32] reported maximum As capture on CaO at 1000 °C. However, CaSO₄ can also retain As [57] and when CaSO₄ was tested for As retention [55], the retention efficiency increased with an increasing temperature from 750 to 1050 °C. Therefore, high temperatures in the fluidized bed (850 °C) might be more favorable for As capture on CaO and notably on CaSO₄ (while the efficiency of Fe-minerals is lower at higher temperatures). Moreover, the SO₃ concentration in non-magnetic residues is higher (10–24%) than that in magnetic fractions (1–2% in the first-step concentrate and 3–7% in manually separated concentrate).

4. Conclusions

Magnetic separation is a widely accepted method used to separate coal ash into two basic components: magnetic and non-magnetic fractions, thereby facilitating their utilization when processed separately. Due to the desulphurization additives added to coal during the fluidized-bed combustion, non-magnetic fractions often contain elevated CaO contents while magnetic concentrates are rich in Fe₂O₃. Both these components are known for their ability to bind As during combustion, whose distribution is a crucial parameter in terms of the utilization of both these fractions. Therefore, this study investigated the As partitioning within magnetic and non-magnetic fractions of fluidized-bed coal combustion ashes.

For a detailed elucidation, two different (successive) procedures of dry magnetic separation were used to separate each sample into strongly magnetic, less magnetic, and non-magnetic fractions. Magnetic concentrates originating from the first separation step (in the vibrofluidized state) contained 60–70% Fe₂O₃, magnetic concentrates separated manually from the residues after the first separation contained 26–41% Fe₂O₃, and the non-magnetic residues contained 2.4–3.5% Fe₂O₃.

Arsenic levels were the highest in the non-magnetic residues (and gradually decreased with an increasing Fe₂O₃ content in the magnetic fractions). The dominant arsenic association in the studied samples was to CaO ($r = +0.909$) and with SO₃ ($r = +0.906$), which is in line with the abundant occurrence of anhydrite identified by XRD analysis. The distribution of Fe₂O₃ and CaO was substantially different ($r = -0.923$), which agrees with the absence of the joint mineral of Fe₂O₃ and CaO by XRD. Instead, the association of Fe₂O₃ and MgO was documented both by a high correlation coefficient ($r = +0.960$) and by identification of magnesioferrite.

Magnetic separation of the ashes is usually conducted with the aim to facilitate the utilization of magnetic and non-magnetic fractions separately. In the case of the samples studied herein, As was depleted in magnetic fractions in relation to non-magnetic ones. It means that if strongly magnetic concentrates are separated from such ash, their As concentrations are decreased to one-third of the As levels in the non-magnetic fractions. Less magnetic fractions contain As contents that are two-thirds of the levels in non-magnetic fractions, which enhances their potential for further technological use.

Author Contributions: Conceptualization and resources, L.B.; investigation and data curation, L.B. and F.K.; writing and editing, L.B. and F.K.; visualization, F.K. All authors have read and agreed to the published version of the manuscript.

Funding: This work was supported by the Doctoral grant competition VSB—Technical University of Ostrava, reg. no. CZ.02.2.69/0.0/0.0/19_073/0016945 within the Operational Programme Research, Development and Education under project DGS/TEAM/2020-014 “Material and energy recovery of waste”; by Ministry of Education, Youth and Sports of the Czech Republic by project “Research on the management of waste, materials and other products from metallurgical and related sectors” (CZ.02.1.01/0.0/0.0/17_049/0008426) and by project No. SP2021/41. Results were also accomplished using Infrastructure ENREGAT under project No. LM2018098.

Data Availability Statement: The data evaluated in this study are available in the article.

Conflicts of Interest: The authors declare no conflict of interest.

References

1. Dai, S.; Graham, I.T.; Ward, C.R. A review of anomalous rare earth elements and yttrium in coal. *Int. J. Coal Geol.* **2016**, *159*, 82–95. [[CrossRef](#)]
2. Bartoňová, L.; Serenčíšová, J.; Čech, B. Yttrium partitioning and associations in coal-combustion ashes prior to and after their leaching in HCL. *Fuel Process. Technol.* **2018**, *173*, 205–215. [[CrossRef](#)]
3. Dai, S.; Seredin, V.V.; Ward, C.R.; Jiang, J.; Hower, J.C.; Song, X.; Jiang, Y.; Wang, X.; Gornostaeva, T.; Li, X.; et al. Composition and modes of occurrence of minerals and elements in coal combustion products derived from high-Ge coals. *Int. J. Coal Geol.* **2014**, *121*, 79–97. [[CrossRef](#)]
4. Dai, S.; Jiang, Y.; Ward, C.R.; Gu, L.; Seredin, V.V.; Liu, H.; Zhou, D.; Wang, X.; Sun, Y.; Zou, J.; et al. Mineralogical and geochemical compositions of the coal in the Guanbanwusu mine, inner Mongolia, China: Further evidence for the existence of an al (Ga and REE) ore deposit in the Jungar Coalfield. *Int. J. Coal Geol.* **2012**, *98*, 10–40. [[CrossRef](#)]
5. Dai, S.; Xie, P.; Ward, C.R.; Yan, X.; Guo, W.; French, D.; Graham, I.T. Anomalies of rare metals in Lopingian super-high-organic-sulfur coals from the Yishan Coalfield, Guangxi, China. *Ore Geol. Rev.* **2017**, *88*, 235–250. [[CrossRef](#)]
6. Zhao, L.; Dai, S.; Nechaev, V.P.; Nechaeva, E.V.; Graham, I.T.; French, D. Enrichment origin of critical elements (Li and rare earth elements) and a Mo-U-Se-Re assemblage in Pennsylvanian anthracite from the Jincheng Coalfield, southeastern Qinshui Basin, northern China. *Ore Geol. Rev.* **2019**, *115*, 103184. [[CrossRef](#)]
7. Dai, S.; Liu, J.; Ward, C.R.; Hower, J.C.; French, D.; Jia, S.; Hood, M.M.; Garrison, T.M. Mineralogical and geochemical compositions of late Permian coals and host rocks from the Guxu Coalfield, Sichuan province, China, with emphasis on enrichment of rare metals. *Int. J. Coal Geol.* **2016**, *166*, 71–95. [[CrossRef](#)]
8. Glushkov, D.O.; Paushkina, K.K.; Shabardin, D.P. Co-combustion of coal processing waste, oil refining waste and municipal solid waste: Mechanism, characteristics, emissions. *Chemosphere* **2020**, *240*, 124892. [[CrossRef](#)] [[PubMed](#)]
9. Wagner, N.J.; Hlatshwayo, B. The occurrence of potentially hazardous trace elements in five highveld coals, South Africa. *Int. J. Coal Geol.* **2005**, *63*, 228–246. [[CrossRef](#)]
10. Bartoňová, L.; Raclavská, H.; Čech, B.; Kucbel, M. Behavior of Cd during coal combustion: An overview. *Processes* **2020**, *8*, 1237. [[CrossRef](#)]
11. Raclavská, H.; Kantor, P.; Růžičková, J.; Kucbel, M.; Švédová, B.; Slamová, K.; Flodrová, Š.; Juchelková, D. An influence of the fuel type on element behaviour in domestic boilers with respect to the circular economy. *Appl. Sci.* **2021**, *11*, 4980. [[CrossRef](#)]
12. Liu, H.; Pan, W.-P.; Wang, C.; Zhang, Y. Volatilization of arsenic during coal combustion based on isothermal thermogravimetric analysis at 600–1500 °C. *Energy Fuels* **2016**, *30*, 6790–6798. [[CrossRef](#)]
13. Low, F.; Zhang, L. Arsenic emissions and speciation in the oxy-fuel fly ash collected from lab-scale drop-tube furnace. *Proc. Combust. Inst.* **2013**, *34*, 2877–2884. [[CrossRef](#)]
14. Wagner, N.J.; Tlotleng, M.T. Distribution of selected trace elements in density fractionated Waterberg coals from South Africa. *Int. J. Coal Geol.* **2012**, *94*, 225–237. [[CrossRef](#)]
15. Wagner, N.J.; Matiane, A. Rare earth elements in select Main Karoo Basin (South Africa) coal and coal ash samples. *Int. J. Coal Geol.* **2018**, *196*, 82–92. [[CrossRef](#)]
16. Tun, M.M.; Juchelková, D.; Raclavská, H.; Sassmanová, V. Utilization of biodegradable wastes as a clean energy source in the developing countries: A case study in Myanmar. *Energies* **2018**, *11*, 3183. [[CrossRef](#)]
17. Raclavská, H.; Juchelková, D.; Roubíček, V.; Matysek, D. Energy utilisation of biowaste—Sunflower-seed hulls for co-firing with coal. *Fuel Process. Technol.* **2011**, *92*, 13–20. [[CrossRef](#)]
18. Hower, J.C.; Robertson, J.D. Chemistry and petrology of fly ash derived from the co-combustion of western United States coal and tire-derived fuel. *Fuel Process. Technol.* **2004**, *85*, 359–377. [[CrossRef](#)]
19. Raclavská, H.; Matysek, D.; Raclavský, K.; Juchelková, D. Geochemistry of fly ash from desulphurisation process performed by sodium bicarbonate. *Fuel Process. Technol.* **2010**, *91*, 150–157. [[CrossRef](#)]

20. Scala, F.; Chirone, R.; Meloni, P.; Carcangiu, G.; Manca, M.; Mulas, G.; Mulas, A. Fluidized bed desulfurization using lime obtained after slow calcination of limestone particles. *Fuel* **2013**, *114*, 99–105. [[CrossRef](#)]
21. Wang, C.; Liu, H.; Zhang, Y.; Zou, C.; Anthony, E.J. Review of arsenic behavior during coal combustion: Volatilization, transformation, emission and removal technologies. *Prog. Energy Combust. Sci.* **2018**, *68*, 1–28. [[CrossRef](#)]
22. Yudovich, Y.E.; Ketris, M.P. Arsenic in coal: A review. *Int. J. Coal Geol.* **2005**, *61*, 141–196. [[CrossRef](#)]
23. Badenhorst, C.; Santos, C.; Lázaro-Martínez, J.; Białecka, B.; Cruceru, M.; Guedes, A.; Guimarães, R.; Moreira, K.; Predeanu, G.; Suárez-Ruíz, I.; et al. Assessment of graphitized coal ash char concentrates as a potential synthetic graphite source. *Minerals* **2020**, *10*, 986. [[CrossRef](#)]
24. Valeev, D.; Kunilova, I.; Alpatov, A.; Varnavskaya, A.; Ju, D. Magnetite and carbon extraction from coal fly ash using magnetic separation and flotation methods. *Minerals* **2019**, *9*, 320. [[CrossRef](#)]
25. Vassilev, S.V.; Menendez, R.; Borrego, A.G.; Diaz-Somoano, M.; Rosa Martinez-Tarazona, M. Phase-mineral and chemical composition of coal fly ashes as a basis for their multicomponent utilization. 3. Characterization of magnetic and char concentrates. *Fuel* **2004**, *83*, 1563–1583. [[CrossRef](#)]
26. Dai, S.; Zhao, L.; Peng, S.; Chou, C.-L.; Wang, X.; Zhang, Y.; Li, D.; Sun, Y. Abundances and distribution of minerals and elements in high-alumina coal fly ash from the Jungar power plant, inner Mongolia, China. *Int. J. Coal Geol.* **2010**, *81*, 320–332. [[CrossRef](#)]
27. Savadogo, N.; Messan, A.; Hannawi, K.; Prince Agbodjan, W.; Tsobnang, F. Durability of mortar containing coal bottom ash as a partial cementitious resource. *Sustainability* **2020**, *12*, 8089. [[CrossRef](#)]
28. Gajda, D.; Lutynski, M.; Kujawska, M. Substitution of magnetite in dense medium separation by zinc-lead waste. *IOP Conf. Ser. Mater. Sci. Eng.* **2018**, *427*, 012036. [[CrossRef](#)]
29. Zheng, C.; Deng, J.; Hong, Z.; Wang, G. Prediction model of suspension density in the dense medium separation system based on LSTM. *Processes* **2020**, *8*, 976. [[CrossRef](#)]
30. Jadhav, R.A.; Fan, L.-S. Capture of gas-phase arsenic oxide by lime: Kinetic and mechanistic studies. *Environ. Sci. Technol.* **2001**, *35*, 794–799. [[CrossRef](#)] [[PubMed](#)]
31. Junying, Z.; Yongchun, Z.; Feng, D.; Han-Cai, Z.; Chu-Guang, Z. Preliminary study of trace element emissions and control during coal combustion. *Front. Energy* **2007**, *1*, 273–279.
32. Sterling, R.O.; Helble, J.J. Reaction of arsenic vapor species with fly ash compounds: Kinetics and speciation of the reaction with calcium silicates. *Chemosphere* **2003**, *51*, 1111–1119. [[CrossRef](#)]
33. Wang, J.; Zhang, Y.; Liu, Z.; Norris, P.; Romero, C.E.; Xu, H.; Pan, W.-P. Effect of coordinated air pollution control devices in coal-fired power plants on arsenic emissions. *Energy Fuels* **2017**, *31*, 7309–7316. [[CrossRef](#)]
34. Zhang, Y.; Wang, C.; Li, W.; Liu, H.; Zhang, Y.; Hack, P.; Pan, W. Removal of gas-phase As₂O₃ by metal oxide adsorbents: Effects of experimental conditions and evaluation of adsorption mechanism. *Energy Fuels* **2015**, *29*, 6578–6585. [[CrossRef](#)]
35. Zhang, Y.; Wang, C.; Liu, H. Experiment and mechanism research on gas-phase As₂O₃ adsorption of Fe₂O₃/γ-Al₂O₃. *Fuel* **2016**, *181*, 1034–1040. [[CrossRef](#)]
36. Zhang, K.; Zhang, D.; Zhang, K.; Cao, Y. Capture of gas-phase arsenic by ferrospheres separated from fly ashes. *Energy Fuels* **2016**, *30*, 8746–8752. [[CrossRef](#)]
37. Parzentny, H.R.; Róg, L. Distribution and mode of occurrence of Co, Ni, Cu, Zn, As, Ag, Cd, Sb, Pb in the feed coal, fly ash, slag, in the topsoil and in the roots of trees and undergrowth downwind of three power stations in Poland. *Minerals* **2021**, *11*, 133. [[CrossRef](#)]
38. Yan, R.; Gauthier, D.; Flamant, G. Possible interactions between As, Se, and Hg during coal combustion. *Combust. Flame* **2000**, *120*, 49–60. [[CrossRef](#)]
39. Contreras, M.L.; Arostegui, J.M.; Armesto, L. Arsenic interactions during co-combustion processes based on thermodynamic equilibrium calculations. *Fuel* **2009**, *88*, 539–546. [[CrossRef](#)]
40. Seames, W.S.; Wendt, J.O.L. Regimes of association of arsenic and selenium during pulverized coal combustion. *Proc. Combust. Inst.* **2007**, *31*, 2839–2846. [[CrossRef](#)]
41. Mahuli, S.; Agnihotri, R.; Chauk, S.; Ghosh-Dastidar, A.; Fan, L.S. Mechanism of arsenic sorption by hydrated lime. *Environ. Sci. Technol.* **1997**, *31*, 3226–3231. [[CrossRef](#)]
42. Zhao, Y.; Zhang, J.; Huang, W.; Wang, Z.; Li, Y.; Song, D.; Zhao, F.; Zheng, C. Arsenic emission during combustion of high arsenic coals from southwestern Guizhou, China. *Energy Convers. Manag.* **2008**, *49*, 615–624. [[CrossRef](#)]
43. López-Antón, M.A.; Díaz-Somoano, M.; Spears, D.A.; Martínez-Tarazona, M.R. Arsenic and selenium capture by fly ashes at low temperature. *Environ. Sci. Technol.* **2006**, *40*, 3947–3951. [[CrossRef](#)] [[PubMed](#)]
44. Fu, B.; Liu, G.; Sun, M.; Hower, J.C.; Mian, M.M.; Wu, D.; Wang, R.; Hu, G. Emission and transformation behavior of minerals and hazardous trace elements (HTEs) during coal combustion in a circulating fluidized bed boiler. *Environ. Pollut.* **2018**, *242*, 1950–1960. [[CrossRef](#)] [[PubMed](#)]
45. Areeprasert, C.; Scala, F.; Coppola, A.; Urciuolo, M.; Chirone, R.; Chanyavanich, P.; Yoshikawa, K. Fluidized bed co-combustion of hydrothermally treated paper sludge with two coals of different rank. *Fuel Process. Technol.* **2016**, *144*, 230–238. [[CrossRef](#)]
46. Ohenoja, K.; Pesonen, J.; Yliniemi, J.; Illikainen, M. Utilization of fly ashes from fluidized bed combustion: A review. *Sustainability* **2020**, *12*, 2988. [[CrossRef](#)]
47. Bartoňová, L.; Klika, Z. Effect of CaO on retention of S, Cl, Br, As, Mn, V, Cr, Ni, Cu, Zn, W and Pb in bottom ashes from fluidized-bed coal combustion power station. *J. Environ. Sci.* **2014**, *26*, 1429–1436. [[CrossRef](#)] [[PubMed](#)]

48. Bartoňová, L. Unburned carbon from coal combustion ash: An overview. *Fuel Process. Technol.* **2015**, *134*, 136–158. [[CrossRef](#)]
49. Parzenty, H.R.; Róg, L. Distribution of some ecotoxic elements in fuel and solid combustion residues in Poland. *Energies* **2020**, *13*, 1131. [[CrossRef](#)]
50. Clemens, A.H.; Damiano, L.F.; Gong, D.; Matheson, T.W. Partitioning behaviour of some toxic volatile elements during stoker and fluidised bed combustion of alkaline sub-bituminous coal. *Fuel* **1999**, *78*, 1379–1385. [[CrossRef](#)]
51. Zhao, S.; Duan, Y.; Chen, C.; Wu, H.; Liu, D.; Liu, M.; Lu, J.; Gu, X. Distribution and speciation transformation of hazardous trace element arsenic in particulate matter of a coal-fired power plant. *Energy Fuels* **2018**, *32*, 6049–6055. [[CrossRef](#)]
52. Zhang, W.; Sun, Q.; Yang, X. Thermal effects on arsenic emissions during coal combustion process. *Sci. Total Environ.* **2018**, *612*, 582–589. [[CrossRef](#)]
53. Díaz-Somoano, M.; López-Antón, M.A.; Huggins, F.E.; Martínez-Tarazona, M.R. The stability of arsenic and selenium compounds that were retained in limestone in a coal gasification atmosphere. *J. Hazard. Mater.* **2010**, *173*, 450–454. [[CrossRef](#)] [[PubMed](#)]
54. Ohki, A.; Nakajima, T.; Sakaguchi, Y.; Iwashita, A.; Takanashi, H. Analysis of arsenic and some other elements in coal fly ash by x-ray photoelectron spectroscopy. *J. Hazard. Mater.* **2005**, *119*, 213–217. [[CrossRef](#)] [[PubMed](#)]
55. Chen, D.; Hu, H.; Xu, Z.; Liu, H.; Cao, J.; Shen, J.; Yao, H. Findings of proper temperatures for arsenic capture by CaO in the simulated flue gas with and without SO₂. *Chem. Eng. J.* **2015**, *267*, 201–206. [[CrossRef](#)]
56. Li, Y.; Tong, H.; Zhuo, Y.; Li, Y.; Xu, X. Simultaneous removal of SO₂ and trace As₂O₃ from flue gas: Mechanism, kinetics study, and effect of main gases on arsenic capture. *Environ. Sci. Technol.* **2007**, *41*, 2894–2900. [[CrossRef](#)]
57. Yang, Y.; Hu, H.; Xie, K.; Huang, Y.; Liu, H.; Li, X.; Yao, H.; Naruse, I. Insight of arsenic transformation behavior during high-arsenic coal combustion. *Proc. Combust. Inst.* **2019**, *37*, 4443–4450. [[CrossRef](#)]